Quartz Tuning Fork Sensor

Mikhail Yakovlev
Physics Department, Kwantlen Polytechnic University,
Richmond, British Columbia, Canada
(Dated: April 2022)

I. Introduction

The aim of the project is to develop a sensor utilizing a quartz tuning fork (QTF) as the sensing element. The end goal of the project is to have an autonomous and reliable sensor capable of measuring change in ambient conditions (ex. microtopography [1], temperature [2][3], gaseous analytes[4][5]). Developing the sensor entails building an electric circuit incorporating the QTF, and also the ability to interpret QTF output signal for sensing purposes

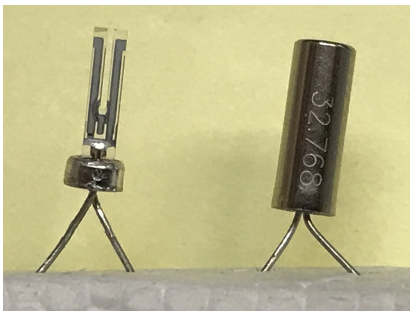

Fig. 1. Photo of a QTF out of (left) and inside (right) the sealed can.

A. Physics of Quartz Tuning Forks

A QTF (Fig. 1) is a tuning fork resonator cut from quartz crystal. The tuning fork itself is a mechanical oscillator, that could be represented as mass m on spring with constant k and damping b with force being applied to it (Fig. 2 & Eq. 1) [1];

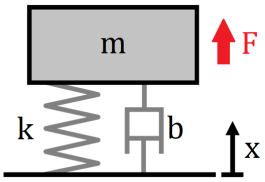

Fig. 2. Diagram of a mechanical oscillator: force F applied to mass m on spring with constant k and damping b causes displacement x.

$$F(t) = m\ddot{x}(t) + b\dot{x}(t) + kx(t) \tag{1}$$

Other than being a mechanical oscillator, QTFs possess piezoelectric properties of quartz crystal. Application of voltage to quartz crystal results in mechanical strain (sets the tuning fork in motion); at the same time, the deformation of crystal during the oscillation produces an electric signal of its own. Therefore, QTF may also be considered as an electronic oscillator: inductor L, capacitor C, and resistor R placed in series (Fig. 3 & Eq. 2) [1]. By comparing Eq. 1 & Eq. 2, an analogy between two representations may be drawn: L corresponds to m, R to b, and C^{-1} to k. Consequently, any alteration of the mechanical properties of the QTF is to be reflected as a change in the electric signal coming from QTF.

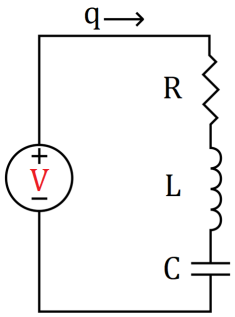

Fig. 3. Diagram of an electronic oscillator: AC voltage source V facilitates the flow of charge q across indicator L, capacitor C, and resistor R.

$$V(t) = L\ddot{q}(t) + R\dot{q}(t) + C^{-1}q(t) \tag{2}$$

B. Electronic Resonator Signal

Since QTF is a resonator, the output signal is dependant on the frequency of the supplied voltage (Eq. 3). At resonant frequency f_0 (Eq. 4), the L and C^{-1} impedance terms cancel out, leaving only R and causing the output current to be at its possible maximum, often referred to as the resonant peak (Fig. 4). Moreover, due to the presence of L and C in the model, off-resonance QTFs produce signal which has phase-difference when compared to the input voltage (Fig. 5); at resonance however, the phase-difference is equal to zero. Since the amplitude of resonance peak (its maximum value) is dependant on the ambient conditions (mostly regarding b), the fact that phase-difference is zero at resonance will be used for sensing purposes.

$$I = \frac{V}{\sqrt{R^2 + (\omega L - \frac{1}{\omega C})^2}} \tag{3}$$

$$f_0 = \frac{\omega_0}{2\pi} = \frac{1}{2\pi\sqrt{LC}} \tag{4}$$

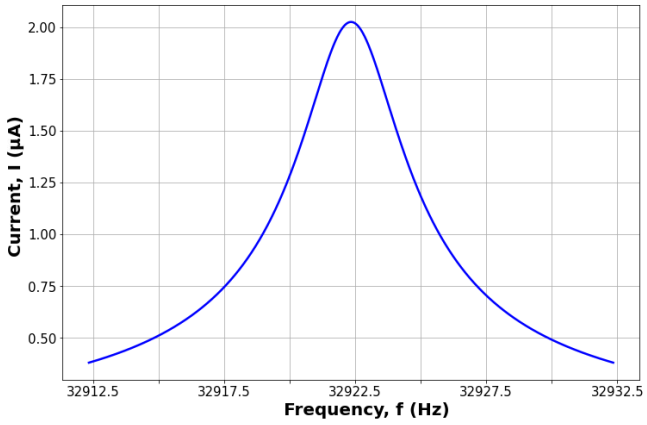

Fig. 4. Resonance peak in current response of an ideal QTF (mathematical model built in Python). Inductor L = 20.5kH, resistor R = 494kΩ, capacitor $C = 1.14$fF [6]; supplied voltage$V$ = 1V.

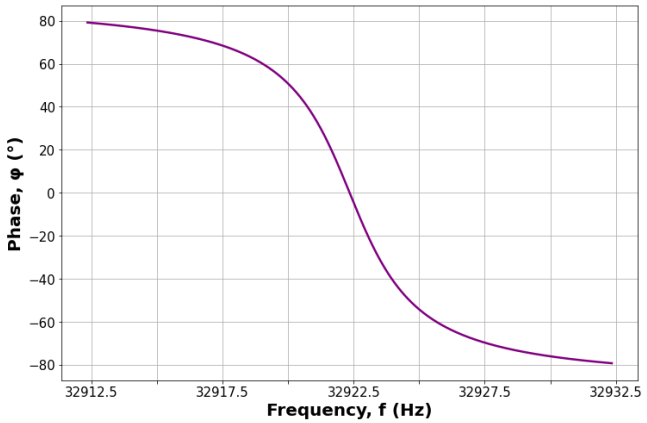

Fig. 5. Phase-difference between output current and input voltage signals in an ideal QTF (mathematical model built in Python). Inductor L = 20.5kH, resistor R = 494kΩ, capacitor $C = 1.14$fF [6]; supplied voltage$V$ = 1V.

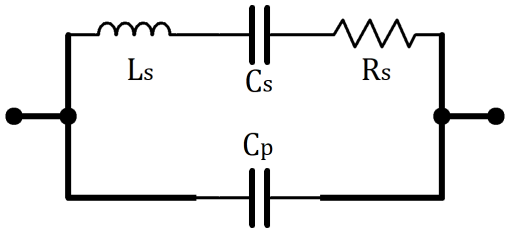

Fig. 6. Diagram of real-life QTF: parasitic capacitance C_p placed in parallel to the series $L_s C_s R_s$ components/

The current output equation of the system must also be enhanced to account for C_p (Eq. 5, Appendix A). Examination of the equation, combined with the data from physical QTF (Fig. 7), concludes that the consideration of C_p in the system results in development of stray-resonant dip in the signal curve at frequency f_p (Eq. 6). It is necessary to neutralize the effect of stray capacitance, as the purely electric signal from stray "capacitor" C_p combines with mechanical signal of the QTF; such combination is detrimental to the sensor application centred around change in mechanical properties of the fork.

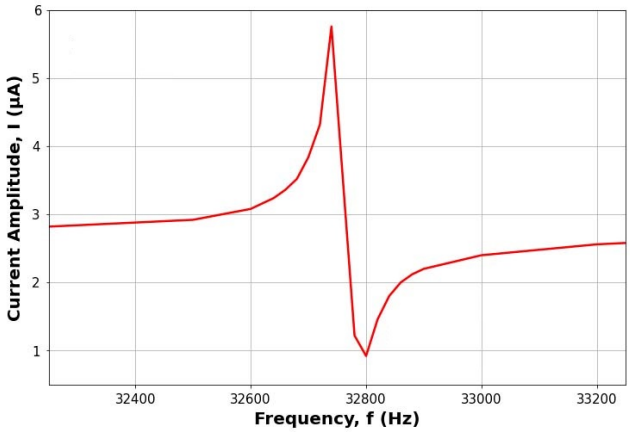

Fig. 7. Coarse frequency sweep of in-the-can QTF (supplied voltage = 1.0V).The curve posses frequency peak at $f_0 = 32.74$kHz and frequency dip at 32.78kHz.

II. Stray Capacitance

A. Overview

The electronic oscillator model does not represent a real-life QTF completely. The metal plating on the surface of QTF and the leads supplying the drive voltage are sources of stray capacitance. Thus, the model should be modified by placing a capacitor C_p, representing stray capacitance, in parallel to the established series inductor, resistor, and capacitor (labeled L_s, R_s, and C_s respectively to prevent confusion; Fig. 6).

$$I = V(Z_{C_p}^{-1} + (Z_{L_s} + Z_{R_s} + Z_{C_s})^{-1})$$

$$= \frac{V\sqrt{R_s^2 + (\omega^3 L_s^2 C_p + \omega R_s^2 C_p + \frac{C_p}{\omega C_s^2})^2 + \frac{1}{\omega C_s} - \omega L_s - \frac{2\omega L_s C_p}{C_s}}}{R_s^2 + (\omega L_s - \frac{1}{\omega C_s})^2} \quad (5)$$

$$f_p = f_s\sqrt{1 + \frac{C_s}{C_p}} \quad (6)$$

B. Compensation

A way to circumvent parasitic capacitance is to cancel the current from C_p. This in turn requires introduction of

a physical capacitor C_c parallel to the QTF [6] (both series $L_s C_s R_s$ and C_p) and powering it with an equal and opposite voltage to that of the QTF (Fig. 8).

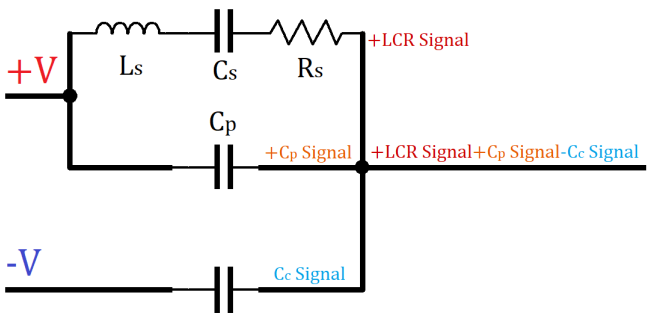

Fig. 8. Diagram of C_p compensation: compensating capacitor C_c is powered oppositely to C_p and $L_s C_s R_s$.

The inclusion of C_c, the total current equation also requires adjustment (Eq. 7, Appendix B). By inspection, if C_c is equal to C_p, the additional capacitance term will cancel each other out, simplifying the equation down to classic LCR circuit current (Eq. 3. In order to account for various source of stray capacitance (not only the QTF plating) C_c was chosen to be a trimmer capacitor, allowing to adjust compensation for the circuit model in progress.

$$I = V(Z_{C_p}^{-1} + (Z_{L_s} + Z_{R_s} + Z_{C_s})^{-1} - Z_{C_c}^{-1})$$

$$= \frac{V\sqrt{R_s^2 + (\omega L - \frac{1}{\omega C_s} + (C_p - C_c)(\omega^3 L^2 + \frac{1}{\omega C_s}^2 + \omega R_s^2 - \frac{2L_s\omega}{C_s}))^2}}{R_s^2 + (\omega L_s - \frac{1}{\omega C_s})^2} \quad (7)$$

III. Lock-In Amplifier

Lock-in amplifier (LIA) is a phase sensitive detector capable of comparing two waveform signals and determine the phase-difference between them. The comparison is performed through multiplication of the reference signal and and the signal in question, and analyzing the average value of the resultant wave signal (Fig. 9).

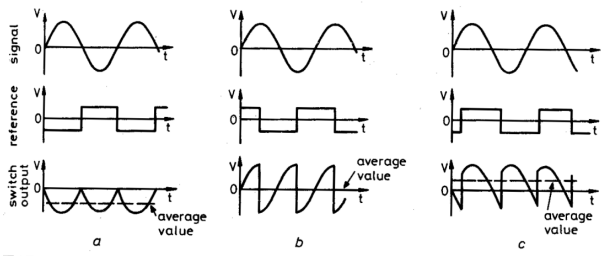

Fig. 9. Waveforms in a phase-sensitive detector for different phase conditions: a) ϕ = 180°; b) ϕ = 90°; c) arbitrary phase [7].

Since the change in the average value of output needs only to be phase dependant, the reference signal needs to be constant amplitude and sharp transition around 0V. This is best achieved with a square-wave signal $V_R(t)$ (Eq. 8). Assuming that the analyzed signal $V_S(t)$ is sinusoidal (Eq. 9), and that frequencies ω_R and ω_S are equal, the multiplication output V_ϕ (Eq. 10 [7]) becomes dependant on the phase of the signals (ϕ_R and ϕ_S), magnitude of input voltage A_s and magnitude of zero-frequency response A_0 (LIA is equipped with low-pass filter, frequencies above ω_R are eliminated).

$$V_R(t) = \frac{4}{\pi}[cos(\omega_R t + \phi_R) - \frac{cos(3\omega_R t + 3\phi_R)}{3} + \frac{cos(5\omega_R t + 5\phi_R)}{5} - \frac{cos(7\omega_R t + 7\phi_R)}{7} + ...] \quad (8)$$

$$V_S(t) = \frac{1}{\sqrt{2}} A_S cos(\omega_S t + \phi_S) \quad (9)$$

$$\begin{aligned} V_\phi &= V_R(t)V_S(t) \\ &= \frac{2\sqrt{2}A_S}{\pi}[cos(\omega_R t \pm \omega_S + \phi_R \pm \phi_S) \\ &\quad - \frac{cos(3\omega_R t \pm \omega_S + 3\phi_R \pm \phi_S)}{3} \\ &\quad + \frac{cos(5\omega_R t \pm \omega_S + 5\phi_R \pm \phi_S)}{5} \\ &\quad - \frac{cos(7\omega_R t \pm \omega_S + 7\phi_R \pm \phi_S)}{7} + ...] \\ &= \frac{2\sqrt{2}A_S A_0}{\pi} cos(\phi_R - \phi_S) \end{aligned} \quad (10)$$

IV. PI Controller

Control loop allows to employ feedback signal for modulation in the system. In this project, feedback signal would be V_ϕ modulating frequencies of the entire circuit. Change in ambient conditions would result in V_ϕ changing, causing the circuit adjust its operating frequency. As the new resonance is being approached to, V_ϕ would decrease, eventually becoming zero at equilibrium (phase-locked loop locked to 0°phase-difference). In such setup the operating frequency of the circuit would be used to measure ambient variable.

Per control theory, it is recommended to utilize all proportional (P), integral (I), derivative (D) gains in feedback modulation. However, for the purposes of this project, D gain will be omitted, as it only improves settling time in the system which is of low concern at early stages of sensor development. The following components will be comprising the PI control unit, all using operational amplifier (OpAmp) as the baseground:

A. Differential Amplifier

Differential amplifier (Fig. 10) will serve the purpose of comparing V_ϕ to the set point signal V_{set}. The output of the amplifier V_{dif} is described by Eq. 11. Given that the resistors are all equal, Eq. 11 simplifies down to being the difference of V_set and V_phi. The unit allows to confirm the completeness of feedback loop.

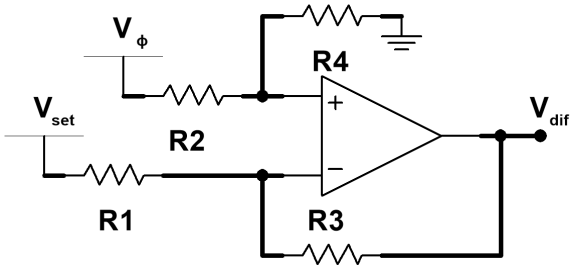

Fig. 10. Diagram of a differential amplifier.

$$V_{dif} = -V_{set}\left(\frac{R_3}{R_1}\right) + V_\phi\left(\frac{R_4}{R_2+R_4}\right)\left(\frac{R_1+R_3}{R_1}\right) \quad (11)$$

B. Proportional Amplifier

Proportional amplifier provides P gain within the controller. In order to have best ability in regulating the P gain, inverting amplifier (Fig. 11 & Eq. 12) was chosen to provide P gain.

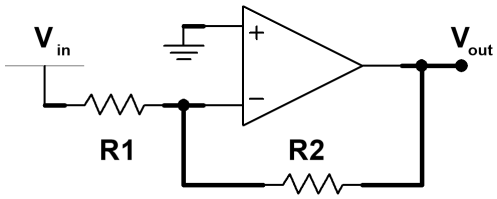

Fig. 11. Diagram of an inverting amplifier.

$$V_{out} = -V_{in}\left(\frac{R_2}{R_1}\right) \quad (12)$$

C. OpAmp Integrator

OpAmp Integrator (Fig. 12) provides I gain to the system. Since capacitor C_F is a time-dependant component in the circuit, the output of the amplifier can be described per Eq. 13 [8], with time constant $\tau = R_I C_F$. Although classic integrator circuit requires only C_F in the OpAmp feedback, additional resistor R_F will be introduced "stable biasing"[8] (R_F needs to be larger than input resistor R_I).

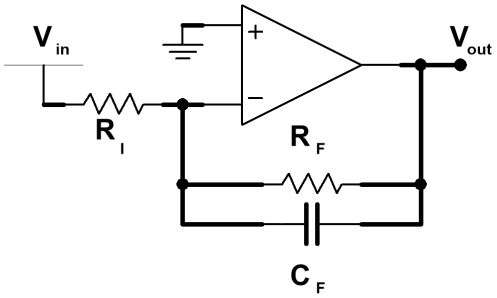

Fig. 12. Diagram of an OpAmp integrator.

$$V_{out}(t) = -V_{in}\frac{1}{R_I C_F}\int V_{in}(t)dt \quad (13)$$

D. OpAmp Summer

OpAmp summer (Fig. 13 & Eq. 14) brings the P and I signals back together to be further used as modulation signal. Since no additional amplification is desired, all resistors in the summer will be kept equal.

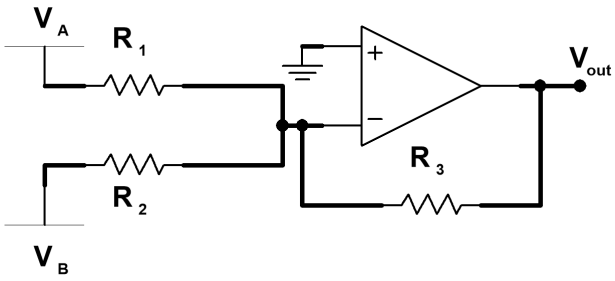

Fig. 13. Diagram of an OpAmp summer.

$$V_{out} = -\left(V_A\frac{R_3}{R_1} + V_B\frac{R_3}{R_2}\right) \quad (14)$$

V. Phase-Locked Loop Development

A. Center-Tapped Transformer Compensation

First stage of the development of the sensor circuit was to make a system for C_p compensation, the major part of which is supplying equal and opposite voltages to QTF and C_c. To achieve that a center-taped transformer (CTT) was used [6]. Due to the secondary coil being grounded in the middle, CTT outputs are opposite with equal magnitude (half of the voltage across primary coil). In order to have better control over C_c, two trimmer capacitor were placed in series allowing for finer capacitance adjustment.

Since the output of the compensating unit is current, a trans-impedance amplifier (TIA, Fig. 14) was introduced [6]. Per Eq. 15, TIA effectively converts current I_{in} to voltage V_{TIA}, with a capability of performing signal amplification (depends on the size of the resistor R_F).

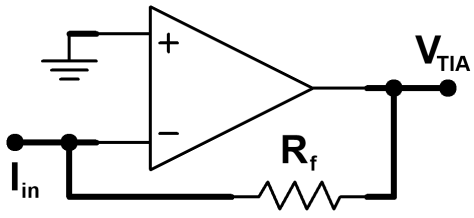

Fig. 14. Diagram of a TIA.

$$V_{TIA} = I_{in}R_f \quad (15)$$

Initial attempts at successful compensation were performed with the circuit being powered by function generator (FG) output of TIA being connected to oscilloscope (OSC). Changing resonance around 32.75kHz resulted in variation of the output wave amplitude on OSC. Adjustment of C_c resulted in the pre- and post-peak drop-offs having different rates. To achieve complete compensation, the following method was developed:

1) Determine the f_0 by observing the amplitude of the output (V_{TIA} would be at its possible maximum);
2) Check the amplitude of the amplitude of V_{TIA} at $\pm$ 1Hz around f_0;
3) If the difference is significant, adjust C_c to reduce the observed difference;
4) Continue performing the procedure until the difference is reduced to acceptable level;

B. Lock-In Amplifier

OSC trials demonstrated necessary success in order to proceed to LIA introduction. For the reference signal, FG's *Sync Out* output was used, providing the square wave signal to LIA. it was discovered that the LIA used could not only determine the phase-difference, but also the amplitude of the input signal, allowing for significantly more accurate adjustment of C_c to achieve complete compensation.

Fig's. 15 & 16 were collected to demonstrate the C_p compensation. Fig. 15 demonstrates a prominent resonant peak with a minor difference between the peak sides. The phase-difference around f_0 (Fig. 16) was found to be very symmetrical as well, with minimal amount of curvature to it. Therefore, relationship between phase-difference and frequency was approximated to being linear; extended sweep found the linear approximation extends to $\pm$2.5Hz around f_0.

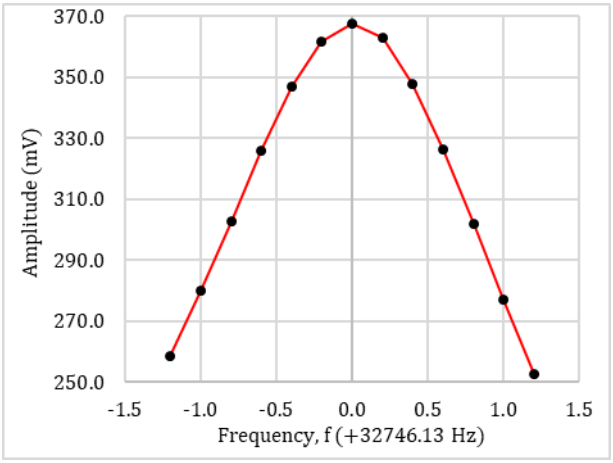

Fig. 15. Resonant peak data collected with LIA for QTF with completely compensated of C_p.

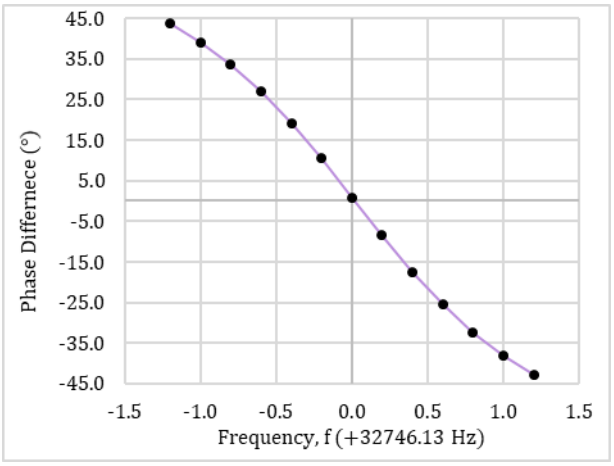

Fig. 16. Phase-difference data collected with LIA for QTF with completely compensated of C_p.

C. PI Controller

Based on initial designs (Fig's. 10 - 13), PI controller was assembled with minor modifications (Fig. **??**). Upon first connection, the output of the controller was found to have exceptional levels of noise. Two decoupling capacitors were placed on both of the powering rails in order to reduce the mentioned noise. Additionally, potentiometer was added to OpAmp integrator to allow for zeroing OpAmp offset.

D. Frequency Modulation

Prior to performing tests on completed phase-locked loop, it was necessary to become familiar with frequency modulation (FM) in FG. The modulation is performed according to Eq. 16, where the operating frequency f_{MOD} depends on the on the fraction of input modulation voltage V_{MOD} to the modulation voltage limit V_{max} (instrument dependant); the fraction is multiplied by frequency deviation Δf, and corresponds to frequency shift around centre frequency f_{centre} (at $\pm V_{max}$, $f_{MOD} = f_{centre} \pm \Delta f$).

$$f_{MOD} = f_{centre} + \frac{V_{MOD}}{V_{max}} \Delta f \tag{16}$$

However, it is necessary to confirm the expected modulation behaviour. An experiment was setup (Fig. 17), where FG#1 was programmed to output DC voltage of varying offset (-6.0 to +6.0 V). The output of FG#1 was used as modulation signal for FG#2 (the FG that would be used in phase-locked loop). FG#2 was set into FM mode with f_{centre} and Δf being recorded. Finally, FG#2 output is fed to OSC for the measurement; through instrument programming, code (Appendix C, [9]) acquired the frequency of the waveform of OSC to store in a data file.

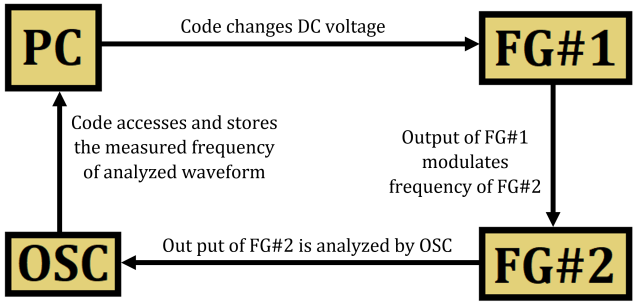

Fig. 17. Block-diagram of FM verification experiment.

Fig. (Fig. 18) is the result of FM verification experiment. It was shown that FM extends beyond manufacturer stated V_{max} =5.0V (from -5.3 to +5.6V). Also the 0V frequency was measured to be different from the specified f_{centre}. The measured FM slope was 0.4545 Hz/V instead of 0.5000 Hz; this means that measured $\Delta f = 2.2725$Hz rather than expected 2.500Hz.It is important to note that the observed results may combine the imperfection of both FG#2 (since it is being modulated) and OSC used (since it is used to acquire f_{MOD}, as FG does not have ability to track the value).

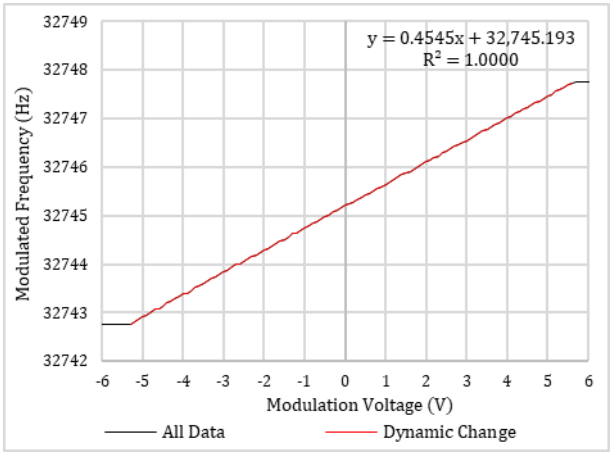

Fig. 18. Calibration of the function generator's frequency modulation mode for f_{centre} = 32745.000Hz. The linear fit equation $f_{MOD} = V_{MOD} \times$ 0.4545Hz/V+32745.193Hz for the dynamic range of -5.3V to +5.6V.

These results were not consequently used for improving the setup, as at the current stage in development process it is important to verify the fundamental principle of sensor working. However, it would be important to account for the mentioned deviations at the final stages of development, such as supporting code that would acquire operating frequency value from the phase locked loop.

E. Sine-to-Square Converter

First attempts to run the phase-locked loop were unsuccessful. Phase-difference on LIA was cyclic (-180°to +180°). It was later discovered that FM affected only main channel output of FG, as *Sync Out* could not be modulated. To resolve this problem, an alternative method of reference square wave generation was proposed: OpAmp saturation (Fig. 19). The OpAmp saturates V_{in} to the value of corresponding powering voltage (Eq. 17). Therefore, sine wave that passed through the OpAmp can be approximated as a square wave that could be used as reference signal in LIA. The rate of saturation is highly dependable on the amplitude of the input; it was observed that no significant change in saturation rate when V_{in} is half or greater of the powering voltages.

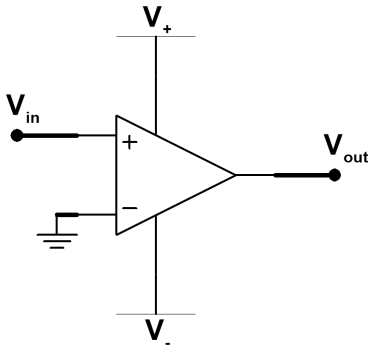

Fig. 19. Diagram of a saturating OpAmp.

$$V_{out} = V_+ \quad \text{if} \quad V_{in} > 0; \qquad = V_- \quad \text{if} \quad V_{in} < 0 \tag{17}$$

Introduction of saturating OpAmp caused another set of problems:

1) The OpAmp had significantly higher input impedance which interfered with the working of compensating unit;
2) Sharp square wave requires V_{in} to be high, but applying the same voltage to QTF may damage the crystal;

The resolution of the problem was found as a buffer amplifier (inverting amplifier with gain>-1, Fig. 11 with $R_1 > R2$) before the compensating unit (Fig. 20). The OpAmp equalizes input impedance, and dropping the voltage prevents damaging of QTF.

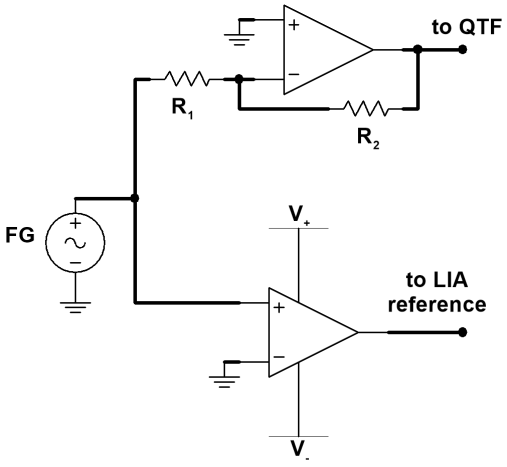

Fig. 20. Diagram of a saturating OpAmp and OpAmp "dropper" in phase-locked loop.

F. Circuit Assembly

In order to reduce the length of wiring and reduce potential sources of additional capacitance within the sensor circuit, the circuit was transferred from breadboards to a single circuit board. However, during verification of the circuit, it was found that additional AC noise signals became noticeable, specifically 60Hz and 50kHz signals. Assuming the 60Hz signal is electric noise, as shielding aluminum box was made, with connections to the circuit being made through BNC connectors in the wall of the box. Repeated tests showed that the electric noise was eliminated, but 50kHz noise remained. Further investigation suggested that 50kHz is the new resonance of the circuit with extremely wide (several kHz) resonant peak, while the expected sharp 32.76kHz resonance disappeared. The origin of the new resonance is suspected to be CTT, as being coils in the transformer possess capacitance, inductance, and resistance, making it an oscillator as well.

G. Dual OpAmp Compensation

In order to circumvent the problem, CTT was removed with a new method of providing equal-and-opposite voltages: dual OpAmp setup (Fig. 21, [10]). Using the combination of these OpAmps allows to power QTF and C_c with equal and opposite voltages (since inverting amplifier has gain<0, and non-inverting amplifier has gain>1, Eq. 18) For simplicity, it was chosen to keep all the resistors in the setup the same, resulting in input QTF signal having -1 gain, and C_c signal having the gain of 2. Therefore, to achieve complete compensation, C_c needs to be only half of C_p.

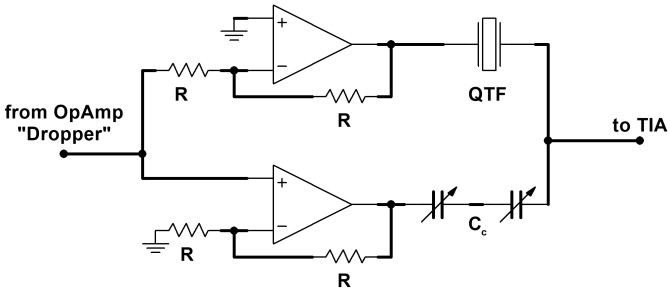

Fig. 21. Diagram two-OpAmp C_p compensation method. Inverting amplifier (top) powers QTF, while non-inverting amplifier (bottom) powers C_c.

$$V_{out} = V_{in}\left(\frac{R_f}{R_i} + 1\right) \tag{18}$$

H. Verification

To verify that the phase-locked loop does perform frequency adjustment, a simple test was performed: an additional FG (reference FG) was connected to differential amplifier (Fig. 21, as V_{set}). Reference FG's waveform was set to be minimal amplitude noise (approximated DC voltage), with the offset being adjusted. Fig. 22 demonstrates the behaviour of the phase-locked loop in response to V_{set} change.

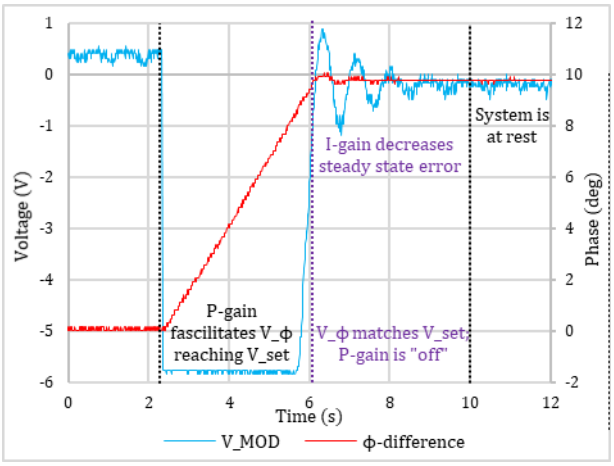

Fig. 22. Data from phase-locked loop verification test, demonstrating the work of PI controller.

As expected, there is a difference in V_{MOD} value between the start and end of the test, indicating that frequency adjustment did occur. The drop in V_{MOD} after 2 seconds indicates that PI controller was working to V_ϕ to match V_{set}. Once matching, the P-gain stops working, and I-gain begins to reduce the steady state error (oscillations). At 10 second mark, the error has been reduced completely, indicating that the loop has reached equilibrium.

The successful verification suggested that the phase locked loop is complete (Fig. 23). PI controller was slightly enhanced during verification process by introducing a low-pass RC filter at the output of OpAmp summer. The filter removed high frequency noises, improving the general noise level of V_{MOD} and bringing down the error in f_{MOD} down to 50mHz.

VI. Air Flow Sensor

Initial method of testing the sensor was placement in pressure-pot. Evacuating air from the pot would cause the drop in pressure, which QTF would pick up, causing phase-locked loop to adjust the operating frequency to new resonance. When attempted, a significant rise in capacitance was observed again (similar to the first assembly). It was chosen to postpone pressure-pot testing, and instead attempt to verify the sensor by placing QTF in a stream of air (Fig. 24). With the prongs of QTF being parallel to the air flow, the force from the stream would be applied in the direction of prong oscillation. That would impede QTF oscillation to some degree, resulting in f_0 changing; it is expected that V_{MOD} would change, while phase-difference would still be at zero.

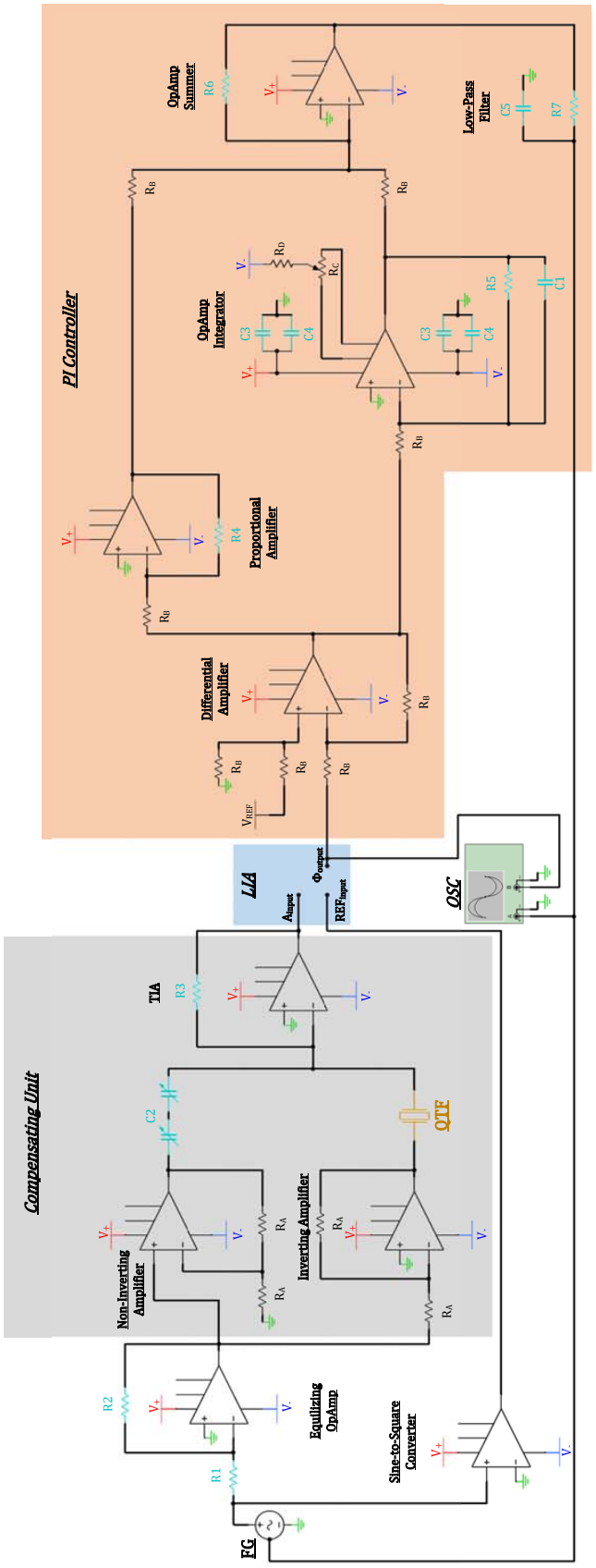

Fig. 23. Diagram of the completed phase-locked loop. Components in cyan are placed with connectors and could be swapped out for different component values. Current component values are: $R_1 = 200\text{k}\Omega$; $R_2 = 10\text{k}\Omega$; $R_3 = 92\text{k}\Omega$; $R_4 = 100\text{k}\Omega$; $R_5 = 10\text{k}\Omega$; $R_6 = 1\text{k}\Omega$; $R_7 = 461\text{k}\Omega$; $R_A = 20\text{k}\Omega$; $R_B = 1\text{k}\Omega$; $R_C = 100\text{k}\Omega$; $R_D = 1.5\text{k}\Omega$; $C_1 = 2.58\text{nF}$; $C_2 = 1.5 - 15\mu\text{F}$; $C_3 = 220\text{nF}$; $C_4 = 10\mu\text{F}$; $C_5 = 10\mu\text{F}$; Appendix D.

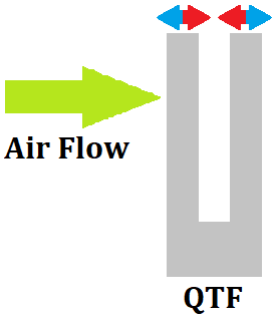

Fig. 24. Diagram of QTF sensor being tested in air flow.

Fig. 25 demonstrates result of air flow sensing. At time of 6s, the air flow valve was slowly opened (as to not damaging QTF). Phase-locked loop reacted to the change by increasing V_{MOD} and causing frequency shift; with ΔV_{MOD} ≈+1V, the corresponding frequency shift is ≈+0.5Hz. At the same time phase-difference experience minimal change (values were converted from V_ϕ. Referring back to Fig. 16, deviation of ≈0.5Hz from normal-condition resonance is expected to result in phase-difference of ≈-20°. Since phase-difference (as observed on LIA) has stayed at zero, the principle of operation for the QTF has been confirmed:

1) QTF is capable of sensing change in environmental conditions that influence its resonance;
2) Phase locked loop is capable of adjusting the operating frequency in real time in response to the change in environment;
3) Once settled, the phase-difference stays at zero, signifying that operating frequency was shifted to the new resonance;

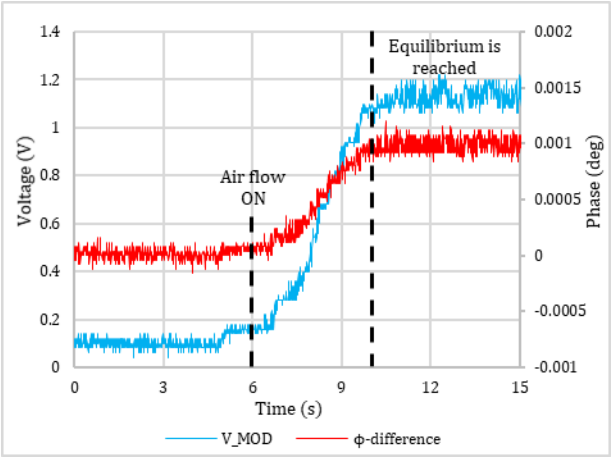

Fig. 25. Response of QTF sensor to being placed inside air flow.

VII. Further Action

With the basic principle of operation confirmed, the next stage of project development would be design improvements and optimization. First step would be optimizing PI gains. Currently, the supposed $\tau = 26\mu$s; however, to prevent ringing in V_{MOD}, time constant of LIA has been set to 10s. Such disparity requires detailed investigation and testing of gains. The goal would be improve the time constant of LIA down to 300ms, yielding a fairly quick responding sensor. Additionally, improvements could be performed on the low-pass filter, to bring the noise levels in V_{MOD} further down (ideally to have error in $f_{MOD} < 10$mHz). This would involve testing combinations of $C5$ and $R7$ (Fig. 23), potentially making the filter multi-staged.

Next, it would be necessary to understand what caused the disappearance of 32.75kHz resonance in first assembly and pressure-pot testing. Currently it is suspected to be caused by increased parasitic capacitance from the length of wires used in the circuit, but there may be additional electromagnetic/electronic influences that are overlooked. The process of tracking down the issue will likely involve re-assembly of the circuit anew, and potentially introducing new components that would stabilize circuit operation. The ultimate goal of the investigation would be to successfully perform pressure-pot testing and observe frequency shift at zero phase-difference.

After that, the project would move in the direction of streamlining the sensor application. Big area of improvement would be miniaturizing the sensor setup, which involves both the circuit and supporting instruments (or finding alternatives alternatives to them). Next big area would be allowing user to have measurements readily available. This would involve further instrument programming for data acquisition, interpretation, graphing etc. For laboratory setting, this would take form of a program with user interface that could be operated from PC without necessary manual interaction with the sensor. Finally, streamlining the sensor could be taken even further by using programmable trimmer capacitors. The end goal would be to have the sensor being able to perform C_p compensation and peak verification automatically (being akin to a zeroing function) through apiece of code.

VIII. Conclusion

A principle phase-locked loop circuit utilizing quartz tuning fork as a sensing element has been built. Sensing is performed on the basis of quartz tuning fork's resonant frequency being dependant on ambient condition that impact prong oscillation. The circuit building began at method development of quartz tuning fork's parasitic capacitance compensation, with the consequent assembly of PI controller for the phase-locked loop. The sensor utilise the principle of zero phase-difference at quartz tuning fork resonance, and uses frequency modulation to perform real time adjustment of operation frequency to the supposed resonance. To verifying sensing capabilities, quartz tuning fork was placed parallel in a stream of air, which would affect prong oscillation; frequency shift of approximately 0.5Hz was observed with phase-difference staying practically at zero. The next steps of development of the circuit would entail circuit optimization, noise reduction, and streamlining sensor operation.

REFERENCES

[1] J-M Friedt and Émile Carry. Introduction to the quartz tuning fork. *American Journal of Physics*, 75(5):415–422, 2007.

[2] Jun Xu, Bo You, Xin Li, and Jing Ma. A high sensitivity quartz tuning fork temperature sensor. pages 616–619, 2009.

[3] Francis Tsow and Nongjian Tao. Microfabricated tuning fork temperature and infrared sensor. *Applied physics letters*, 90(17):174102, 2007.

[4] Xingcai Qin, Xiaojun Xian, Yue Deng, Di Wang, Francis Tsow, Erica Forzani, and Nongjian Tao. Micro quartz tuning fork-based pm 2.5 sensor for personal exposure monitoring. *IEEE Sensors Journal*, 19(7):2482–2489, 2018.

[5] Minghan Ren, Erica S Forzani, and Nongjian Tao. Chemical sensor based on microfabricated wristwatch tuning forks. *Analytical chemistry*, 77(9):2700–2707, 2005.

[6] Robert D Grober, Jason Acimovic, Jim Schuck, Dan Hessman, Peter J Kindlemann, Joao Hespanha, A Stephen Morse, Khaled Karrai, Ingo Tiemann, and Stephan Manus. Fundamental limits to force detection using quartz tuning forks. *Review of Scientific Instruments*, 71(7):2776–2780, 2000.

[7] M. L. Meade. *Lock-in amplifiers: Principles and applications*. P. Peregrinus, 1983.

[8] P. Horowitz and W. Hill. *The art of electronics*. Cambridge University Press, 3 edition, 2015.

[9] Mikhail Yakovlev (YakovMik). Kpu-4thyearproject.

[10] Yexian Qin and R Reifenberger. Calibrating a tuning fork for use as a scanning probe microscope force sensor. *Review of scientific instruments*, 78(6):063704, 2007.

APPENDIX A: CURRENT IN REALISTIC QTF

Current through the realistic QTF (Fig. 6) is described by:

$$I = V/Z$$

where Z is the total impedance of QTF. Since QTF has two parallel branches (series $L_sC_sR_s$ and C_p), parallel impedance formula is applied:

$$Z^{-1} = (Z_{LCR})^{-1} + (Z_{Cp})^{-1}$$

Next we expand the impedance term Z_{LCR}, and replace each individual impedance according to the type of component:

$$Z^{-1} = \left(R_s + j\left(\omega L_s - \frac{1}{\omega C_s}\right)\right)^{-1} + \left(\frac{j}{\omega C_p}\right)^{-1}$$

Combining the terms into a single fraction, with consequent bracket expansion, results in:

$$Z^{-1} = \frac{1 - \omega^2 C_p L_s + \frac{C_p}{C_s} + j\omega C_p R_s}{R_s + j\left(\omega L_s - \frac{1}{\omega C_s}\right)}$$

To get rid off the imaginary component to the equation, we will begin by removing j from the denominator:

$$Z^{-1} = \frac{1 - \omega^2 C_p L_s + \frac{C_p}{C_s} + j\omega C_p R_s}{R_s + j\left(\omega L_s - \frac{1}{\omega C_s}\right)} \times \frac{R_s - j\left(\omega L_s - \frac{1}{\omega C_s}\right)}{R_s - j\left(\omega L_s - \frac{1}{\omega C_s}\right)}$$

$$= \frac{\left[1 - \omega^2 C_p L_s + \frac{C_p}{C_s} + j\omega C_p R_s\right]\left[R_s - j\left(\omega L_s - \frac{1}{\omega C_s}\right)\right]}{R_s^2 + \left(\omega L_s - \frac{1}{\omega C_s}\right)^2}$$

$$= \frac{\left[1 - \omega^2 C_p L_s + \frac{C_p}{C_s} + j\omega C_p R_s\right]\left[R_s - j\left(\omega L_s - \frac{1}{\omega C_s}\right)\right]}{R_s^2 + \left(\omega L_s - \frac{1}{\omega C_s}\right)^2}$$

$$= \frac{R_s + j\left[\omega^3 L_s^2 C_p + \omega R_s^2 C_p + \frac{C_p}{\omega C_s^2} + \frac{1}{\omega C_s} - \omega L_s - \frac{2\omega L_s C_p}{C_s}\right]}{R_s^2 + \left(\omega L_s - \frac{1}{\omega C_s}\right)^2}$$

Finally, Z^{-1} will multiplied by the complex conjugate of itself and square-rooted:

$$\sqrt{Z^{-1} \times \overline{Z}^{-1}} = \left|Z^{-1}\right|$$

$$= \frac{\sqrt{R_s^2 + \left[\omega^3 L_s^2 C_p + \omega R_s^2 C_p + \frac{C_p}{\omega C_s^2} + \frac{1}{\omega C_s} - \omega L_s - \frac{2\omega L_s C_p}{C_s}\right]^2}}{R_s^2 + \left(\omega L_s - \frac{1}{\omega C_s}\right)^2}$$

Therefore, the current through such QTF model would be described as:

$$I = \frac{V\sqrt{R_s^2 + \left[\omega^3 L_s^2 C_p + \omega R_s^2 C_p + \frac{C_p}{\omega C_s^2} + \frac{1}{\omega C_s} - \omega L_s - \frac{2\omega L_s C_p}{C_s}\right]^2}}{R_s^2 + \left(\omega L_s - \frac{1}{\omega C_s}\right)^2} \tag{5}$$

APPENDIX B: CURRENT IN COMPENSATED QTF

Current through the compensated QTF (Fig. 8) is described by:

$$I = V/Z$$

where Z is the total impedance of QTF. Since QTF has two parallel branches (series $L_sC_sR_s$ and C_p), parallel impedance formula is applied:

$$Z^{-1} = (Z_{LCR})^{-1} + (Z_{Cp})^{-1} - (Z_{Cc})^{-1}$$

Next we expand the impedance term Z_{LCR}, and replace each individual impedance according to the type of component:

$$Z^{-1} = \left(R_s + j\left(\omega L_s - \frac{1}{\omega C_s}\right)\right)^{-1} + \left(\frac{j}{\omega C_p}\right)^{-1} - \left(\frac{j}{\omega C_c}\right)^{-1}$$

Combining the terms into a single fraction, with consequent bracket expansion, results in:

$$Z^{-1} = \frac{\omega^2 L_s C_c + \frac{C_p}{C_s} - \frac{C_c}{C_s} - \omega^2 L_s C_p + j\omega R_s C_p - j\omega R_s C_c + 1}{R_s + j\left(\omega L_s - \frac{1}{\omega C_s}\right)}$$

By inspection, it is possible to conclude that in case $C_c = C_p$, all variables in numerator are cancelling out. However in order to have complete expression for current through such circuit, derivation will be continued. First, we remove j from the denominator:

$$Z^{-1} = \frac{\omega^2 L_s C_c + \frac{C_p}{C_s} - \frac{C_c}{C_s} - \omega^2 L_s C_p + j\omega R_s C_p - j\omega R_s C_c + 1}{R_s + j\left(\omega L_s - \frac{1}{\omega C_s}\right)}$$

$$\times \frac{R_s - j\left(\omega L_s - \frac{1}{\omega C_s}\right)}{R_s - j\left(\omega L_s - \frac{1}{\omega C_s}\right)}$$

By term multiplication and expansion, we arrive to the following:

$$Z^{-1} = \frac{R_s + j\left(\omega L_s - \frac{1}{\omega C_s} + [C_p - C_c]\left[\omega^3 L_s^2 + \frac{1}{\omega C_s^2} + \omega R_s^2 - \frac{2\omega L_s}{C_s}\right]\right)}{R_s^2 + \left(\omega L_s - \frac{1}{\omega C_s}\right)^2}$$

Consequently, we multiply Z^{-1} by complex conjugate of itself and taking the square-root to obtain $|Z^{-1}|$. Therefore the expression for current is:

$$I = \frac{V\sqrt{R_s^2 + (\omega L - \frac{1}{\omega C_s} + (C_p - C_c)(\omega^3 L^2 + \frac{1}{\omega C_s}^2 + \omega R_s^2 - \frac{2L_s\omega}{C_s}))^2}}{R_s^2 + (\omega L_s - \frac{1}{\omega C_s})^2} \tag{7}$$

Again, if $C_c = C_p$, a large portion of the equation becomes zero, giving

$$I = \frac{V\sqrt{R_s^2 + (\omega L - \frac{1}{\omega C_s})^2}}{R_s^2 + (\omega L_s - \frac{1}{\omega C_s})^2} = \frac{V}{\sqrt{R_s^2 + (\omega L - \frac{1}{\omega C_s})^2}} \tag{3}$$

APPENDIX C: FREQUENCY MODULATION CONFIRMATION CODE

The code in *FreqVsVolt_Calibration.py* is centered around the use of PyVisa library that allows for communication with VISA interface. The code is meant to be working with Fig. 17 experimental setup.

A. Inputs

The top of the code file contains the list of parameters that could be adjusted by user for optimal verification frequency modulation:

- **FG_name** - VISA name of the individual function generator which will be providing DC signal V_{MOD} (FG#1 on Fig. 17);
- **OSC_name** - VISA name of the individual oscilloscope which be used to acquire the frequency of the modulated function generator (FG#2 on Fig. 17);
- **size** - number of frequency measurements that oscilloscope will be taking per V_{MOD} value;
- **V_max** - the absolute maximum voltage that would be used for modulation, meaning that sweep will be from -V_max to +V_max ;
- **V_delta** - step size in V_{MOD} sweeping;
- **t_delta** - time in seconds between oscilloscope frequency measurements;
- **fwd_bwd_cycles** - total number of forward-backward sweeps that will be performed (one sweep is from -V_max to +V_max to -V_max);

B. Method: Hardware

Prior to using the code ensure instruments are connected per Fig. 17:

- FG#1 is connected to PC;
- Channel #1 of FG#1 is connected to modulation input of FG#2;
- Output channel of FG#2 must be connected to Channel #1 of OSC;
  - Put the chosen output channel of FG#2 into sine waveform with 1V amplitude. Additionally, put the channel into FM of chosen Δf (record it).
- OSC is connected to PC;

Once connections are ensured, the code may be executed and data gathering process will begin.

C. Method: Software

On the software side the following steps are executed in the code:

1) Initialization of libraries and input variables;
2) Determine number of sweep points in signle direction, based on V_max and V_delta;
3) Perform the measurement cycle fwd_bwd_cycles-number of times:
   a) Calculate current V_{MOD} value;
   b) Apply current V_{MOD} to FG#1;
   c) Measure f_{FM} from OSC size-number of times t_delta seconds apart. Calculate average and standard deviation of the just-measured data set. Record the results into a string variable. Perform for every V_{MOD} in current direction;
   d) Save date into .txt file
   e) Repeat the process going in backward direction;

APPENDIX D: EQUIPMENT USED

- **Function Generator**: *RIGOL*'s DG1000;
- **Lock-In Amplifier**: *Stanford Research Systems*' Model SR530;
- **OpAmp**: *Texas Instruments*' TL081CP;
- **Oscilloscope**: *Tektronix*'s TBS1000B/EDU;
- **Quartz Tuning Fork**: *Abracon LLC*'s AB38T-32.768kHz;